Co-design Strategies for Energy-Efficient UWB and UHF Wireless Systems

Alessandra Costanzo, *Senior Member, IEEE*, Diego Masotti, *Senior Member, IEEE*, Marco Fantuzzi, *Student Member, IEEE,* and Massimo Del Prete, *Student Member, IEEE*

(Invited paper)

***Abstract*—This paper reviews the most recent methods, combining nonlinear harmonic-balance-based analysis with electromagnetic (EM) simulation, for optimizing, at the circuit level, modern radiative RF/microwave systems. In order to maximize the system efficiency, each sub-system must be designed layout-wise, accounting for the presence of the others, that is, accounting for its actual terminations, rather than the ideal ones (50 Ohm). In this way, the twofold goal of minimizing size and losses of the system is obtained by reducing inter-system matching networks. Indeed, terminations are complex, frequency-dispersive and variable with the signal level, if active operations are concerned, and are responsible for performance degradation if not properly optimized. This approach is nowadays necessary, given the ever increased spread of pervasively distributed RF microsystems adopting miniaturized antennas, such as radio-frequency identification (RFID) or wireless sensor networks (WSN), that must be low-cost, low-profile, low-power and must simultaneously perform localization, identification and sensing. For the design of a transmitter and a receiver connected with the respective antennas, suitable figures of merit are considered, encompassing radiation and nonlinear performance. Recent representative low-profile realizations, adopting ultra-wideband (UWB) excitations are used to highlight the benefit of the proposed nonlinear/EM approach for next generation energy autonomous microsystem, such as UWB-RFID tags.**

***Index Terms*—Nonlinear simulation, IR-UWB, RFID, energy harvesting.**

I. Introduction

CURRENT RF/microwave micro-systems, integrating antennas, low-power radios and energy harvesting capabilities are receiving an increasing attention, as systems to be pervasively distributed in the ambient for environmental monitoring, objects/people identification and detection, and mobile health [1]-[3]. Such RF systems are required to be compact, low-cost, low profile, and to operate at the lowest possible energy requirements [4], [5]. Furthermore, they are usually required to be energy-autonomous so that they need to integrate energy harvesting (EH) solutions, for immediate use or for recharging on-board batteries [6], [7]. Compactness is achieved by adopting layouts based on multi-layered solutions for the antenna and its feeding network, resulting in transceiver topologies which are not suitable to be described in terms of equivalent circuit models [8], [9]. Thus, stand-alone components' optimization becomes almost useless and it is necessary to adopt techniques able to optimize the performance of each device when it is embedded in its final microwave system implementation, as the puzzle-like interconnection of Fig. 1 highlights. This is true for both the nonlinear sub-circuit and for the antenna; the complex impedance of the latter, has to be included in these system designs directly representing the actual load and source impedances of the transmitter and the receiver, respectively. In this way, the dual advantage of minimizing the components' number and maximizing the overall efficiency is obtained, by reducing the losses, which are significant when micro-power RF systems are involved [10]. Indeed, antenna impedances must be represented as a complex function of frequency rather than as a reference real impedance [6], [11], [12]: and this is true for narrowband systems, that adopt resonant antennas to enhance radiation efficiency, as well as for broad-band and UWB systems, which inevitably arise a complex and variable impedance over the operating band [13], [14]. Furthermore,

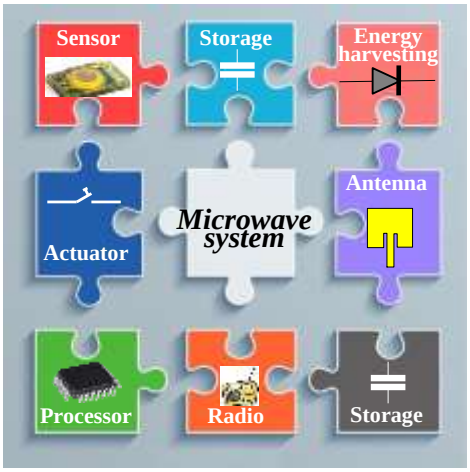

Fig. 1. Pictorial representation of a modern RF/microwave micro-system, integrating radio, antenna, sensor, harvesting unit.

Manuscript submitted October 31, 2017. This work was partly funded by the Italian Ministry of the Instruction, University and Research (MIUR), within the framework of the national project GRETA, and partly by ESA AO 1-8471/15/NL/LvH Localisation of Objects in Space through RF Tags (LOST).

Alessandra Costanzo, Diego Masotti, Marco Fantuzzi, and Massimo Del Prete are with the Department of Electrical, Electronic and Information Engineering, "Guglielmo Marconi," University of Bologna, Italy (email: alessandra.costanzo@unibo.it, diego.masotti@unibo.it marco.fantuzzi3 @unibo.it, massimo.delprete3@unibo.it,).

nonlinearity in the system implies the presence of signal flow at higher order intermodulation products (IM) of the forcing signals, and are normally important inside the circuit having a major influence on several key performance involving power spectral distribution: e.g., RF-dc or dc-RF conversion efficiency, spectral purity, and transducer/conversion gain. Thus, handling harmonics requires both the active devices and the passive subnetwork, including the antennas, to be accurately characterized over a broader frequency band than is normally required for linear applications. Otherwise the derived system design would become sub-optimal or even useless. In recent years, a number of different approaches have been adopted to combine layout-wise nonlinear (NL) simulation tools with EM analysis of the RF linear part [15]-[19]. A first option is to include the circuit nonlinearities into the EM numerical simulation of the linear sub-circuit [18], [19], but, very simple topologies can be analyzed in this way. In a complementary manner, in [17], a time-domain convolution term forces the use of complex strategies to describe the dispersive linear part behavior. When system optimization is concerned, to speed up the overall computation time, artificial neural networks can be adopted, as in [15], [16], to perform efficient NL/EM co-simulation, at the expense of the time-consuming EM analysis for creating, once for all, complex linear subsystems models (such as antennas). In this sense, the space-mapping technique has demonstrated its effectiveness in reducing the EM cost by setting up surrogate models [15], [20].

In this paper, we focus on a more general method for the circuit-level analysis of an entire RF system integrated with its antenna, which allows to directly tackle its performance in terms of radiation characteristics. Indeed, this is the only way to fully account for the antenna influence on the RF circuit performance (including near-field couplings), and for the effects of the circuit layout on the antenna radiation pattern. An interesting aspect of this method is that the design goals may include direct specifications, such as a prescribed radiation intensity. In this way, the radiative behavior of the whole RF system can be tackled directly, for both the receiving and transmitting systems. Proper exploitations of the EM theory are needed to accurately obtain the rigorous model of the radiated power and of the effective received one in the transmitter and receiver, respectively. This approach is particularly important when the focus is on low-power, low-profile micro-systems, adopting UWB and/or ultra-high frequency (UHF) excitation signals, that are the most promising solutions for next generation RFID and Internet of Things (IoT) technologies, integrating EH capabilities. This kind of systems are used as reference examples in this contribution, since the use of UWB backscattered signals offers robustness to indoor interference, thus enhancing passive RFID tags localization accuracy [21]; whereas UHF energy harvesting capabilities become mandatory for sensor/tag energy autonomy, due to the extremely low UWB power budget [22].

The next section, Section II, is dedicated to describe the main simulation strategies to efficiently combine nonlinear and electromagnetic analysis. For the transmitter and the receiver design, different figures of merit are adopted combining nonlinear and radiation performance [8], [11], [23]. In Sections III and IV two demonstrative design examples are detailed. First, the design as a whole of a printed UWB monopole fed by an UWB travelling wave amplifier is addressed, by combining nonlinear Harmonic Balance (HB) - based analysis and full-wave simulation of the resulting active antenna. Second, a compact, reduced-size, single port RFID tag, which combines UWB and UHF operations for simultaneous localization, data and power transfer purposes [4], is presented. Both of them adopt the radiating element as the corresponding load and source termination, respectively. In Section V, the UWB/UHF tag system realization designed for non-conventional microwave substrate, such as paper, is discussed. Finally, Section VI draws a conclusion.

II. Nonlinear-Electromagnetic Co-Simulation of RF Systems

Future 5G architectures [24] envisage the pervasive deployment of IoT devices, consisting of entire RF/microwave micro-systems, always equipped with one or multiple antennas. Their optimum design is very demanding for a twofold reason: i) nonlinearities play an essential role in transceiver operation, since several essential circuit functions, such as signal generation and mixing, are inherently nonlinear. This forces the designer to make use of iterative procedures, and thus to efficiently combine the time-consuming EM analyses with the circuit-level optimization loop. ii) the traditional interface between the antenna and RF circuitry may become questionable, or even meaningless, and the front end can only be correctly represented in terms of a radiative multiport linear subnetwork (including the antenna(s)) described layout-wise, whose ports are connected to the nonlinear devices implementing the indispensable nonlinear circuit functions [25].

In order to design such subsystems (up to the front end level), the combination of nonlinear analysis based on the HB principle with a full-wave characterization of the (possibly radiating) linear subnetwork is the most appropriate strategy to be adopted [15], [16], [26]-[28]. In fact, linear and nonlinear components are described in the proper domain: time-domain for the nonlinearities, and frequency-domain for the linear part (thus accounting for the strongly dispersive behavior of transmission lines and antennas). In particular, the HB technique can rely on two different approaches, the nodal and the piecewise ones: i) in the nodal HB (NHB), the circuit is analyzed as a whole, and the node voltages are chosen as state variables [29]; ii) in the piecewise HB (PHB), the circuit is decomposed into a linear and a nonlinear subnetworks, connected through a set of common ports whose cardinality is (typically) equal to the number of nonlinear device ports; the state variables are (typically) the common port voltages, or quantities related to them [30]. As a consequence, in the NHB case the number of scalar unknowns is significantly larger than in the PHB case. However, the solving matrix of the NHB approach is naturally sparse (because of the sparsity of

the nodal admittance matrix) and can rely upon sparse-matrix techniques. Conversely, the dense nature of this matrix in the PHB approach forces to adopt standard solving techniques (with the exception of artificially induced [31] or augmented sparsity [32] approaches). Typically, the NHB method is more efficient when the majority of the nodes is connected to nonlinear devices (e.g. in MMICs), whereas the PHB method allows the refinement of the linear subnetwork description to any desired extent, without affecting the overall analysis cost. The most advantageous aspect of the PHB method is the unrivaled level of flexibility in the nonlinearities description [30], that allows the straightforward use of non-electrical state variables (e.g., thermal [33], mechanical [34], or unphysical quantities [30]).

Fig. 2 describes the PHB approach in case of a general circuit having a set of N nonlinear device ports, and an antenna or a standard load at the output port. The EM description can be limited to the antenna only, in cases where the adopted frequency and/or the level of integration allow to do it; otherwise it should be extended to the entire linear sub-network.

The aims of the following subsections are: i) to briefly recall the needed HB-based strategies to face the analysis/ design of modern transceivers excited by modulated RF or by UWB signals; ii) to focus the NL/EM approaches for the transmitter- and receiver-side analyses, respectively. In the former case, EM-based figures of merit can be formulated to directly handle the system performance in terms of its actual radiating behavior; in the latter case, the EM theory is exploited to evaluate of the actual available power at the antenna(s) port(s) taking into account the dispersive behavior of the antenna itself.

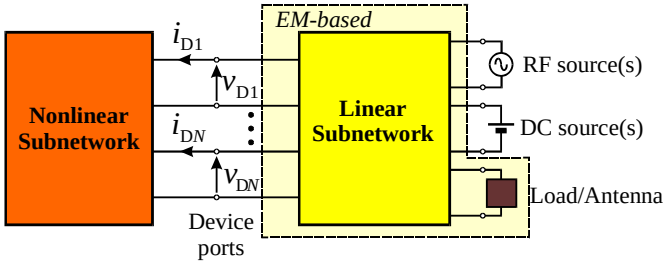

Fig. 2. Generic circuit description according to PHB technique.

A. Harmonic-balance oriented RF system description

Despite of their size, modern transceivers can host a significant number of nonlinear devices (i.e. hundreds). Moreover, the regime of these systems can be quasi-periodic, due to the intermodulation of the input frequencies, or occupy very large bands (if the UWB technology is deployed). As a consequence, in a HB analysis, the predefined multi-tone spectrum $\boldsymbol{K}$ of a generic signal $s(t)$ flowing in the system typically has a high cardinality:

$$s(t) = \mathrm{Re}\left[\sum_{\mathbf{k}\in\mathbf{K}} S_{\mathbf{k}} \exp(j2\pi F_{\mathbf{k}} t)\right] \quad (1)$$

where $F_{\boldsymbol{k}}$ is the generic k-th frequency (or IM product) of the spectrum, and $\boldsymbol{S_k}$ is the k-th complex phasor of the time-signal $s(t)$.

The application, in the frequency domain, of Kirchhoff current law at the device ports for each spectral line, leads to the definition of the HB errors and of the solving system [27]:

$$\boldsymbol{E}(\boldsymbol{X}) = \boldsymbol{I}_{\boldsymbol{L}}(\boldsymbol{X}) + \boldsymbol{I}_{\boldsymbol{NL}}(\boldsymbol{X}) + \boldsymbol{I}_{\boldsymbol{S}} = \boldsymbol{0} \quad (2)$$

where $\boldsymbol{E}$ and $\boldsymbol{X}$ contain the real and imaginary parts of the complex phasors of the HB errors and of the signals (1) adopted as circuit state variables; $\boldsymbol{I_L}(\boldsymbol{X})$ and $\boldsymbol{I_{NL}}(\boldsymbol{X})$ are the vectors of currents flowing into the linear and nonlinear subnetworks, respectively; and, finally, $\boldsymbol{I_S}$ stands for the vector of equivalent excitation sources applied at the device ports. The dimension of (2) can thus become huge, being roughly given by the product of the number of nonlinear device ports and the cardinality of $\boldsymbol{K}$. The use of Krylov subspace model-order-reduction (MOR) [35] brings to dramatic improvements in numerical efficiency (mainly because the system Jacobian matrix does not need to be stored nor factorized), thus offering memory storage and CPU time compatible with ordinary PC requirements.

The simulation of the entire system operating under realistic conditions implies to consider the digital modulation of the driving signal (the RF or IF one, in the reception and transmission operating condition, respectively). This requires the further integration of an envelope-oriented HB algorithm [36]-[38] into the nonlinear/EM co-simulation environment described above, otherwise the circuit analysis would become impractical even with a Krylov-based approach. According to this method, the aperiodic sequence of modulating bits is replaced, for numerical reasons, by a periodic signal generated by periodically repeating a random sequence of N_b bits. The integer N_b must be large enough (i.e. > 1000) to allow the statistical properties of the actual signal to be reproduced by the periodic sequence with sufficient accuracy. The corresponding base-band frequency of the signal is $f_M = B_M/N_b$, where B_M is the bit-rate of the signal. For modern communication standards f_M is orders of magnitude lower than the carrier frequency (f_{RF} or f_{IF}). If this is the case, the envelope-oriented HB algorithm is well-conditioned and directly handles the time-dependent phasors (or envelopes) $\boldsymbol{S_k}(t_M)$ of the generic signal:

$$s(t, t_M) = \mathrm{Re}\left[\sum_{\mathbf{k}\in\mathbf{K}} S_{\mathbf{k}}(t_M) \exp(j2\pi F_{\mathbf{k}} t)\right] \quad (3)$$

where t is the fast carrier (f_{RF} or f_{IF}) time, and t_M is the slow modulating signal or envelope time. The envelope period is then uniformly sampled in a sequence of instants t_m (m=1, 2,…, $M \geq N_b$). An important requirement is that the resulting nonlinear HB system, at a generic envelope sampling instant t_m, has to be backward-coupled to previous states through the envelope dynamics of the system, in order to account for the circuit memory: this can be easily accomplished through a one-sided incremental rule in the evaluation of the state-variables envelope derivatives, given by a linear combination of a number (say 3) of the previously evaluated envelopes [35]. Hence, if we denote by $\boldsymbol{E_m}$ the HB-error vector at the

generic instant t_m, the corresponding HB system becomes:

$$\boldsymbol{E}_m[\boldsymbol{X}(t_m);\boldsymbol{X}(t_{m-1}),\boldsymbol{X}(t_{m-2}),\boldsymbol{X}(t_{m-3})]=\boldsymbol{0} \quad (4)$$

and can be evaluated for all the M instants, but with the same dimension of the non-modulated case, and the preceding envelopes playing the role of parameters.

In cases of extremely large size HB problems (e.g. multiple complex radiating transceivers for Multi-Input Multi-Output (MIMO) applications), the previous algorithms cannot be sufficient to permit the nonlinear/EM co-design with ordinary PCs. More recently, other solutions have been proposed to bridge this gap, by means of a hierarchical procedure [35]: i) the automatic recognition of near-zero spectral components in different portions of the circuit (e.g. in a double-conversion front-end case) allows to perform a first-tier system decomposition, where each portion of the system has its own reduced frequency spectrum; ii) a second-tier automatic decomposition is carried out for each circuit block, by means of the introduction of auxiliary unknowns (the voltages at the block connection ports). Despite of this additional overhead, the *a priori* known sparse structure of the resulting Jacobian matrix allows both a dramatic reduction of the memory occupation, and an incredible reduction of the Krylov MOR calculations, thus achieving analyses two orders of magnitude faster and size-reduced. This method is thus potentially able to obtain the best tradeoff between the NHB and the PHB philosophies, while substantially preserving the peculiar advantages of the latter.

In [39] another smart technique, facing the problem of simulating heterogeneous wireless systems composed of baseband and RF blocks, is proposed: some signals of the system are described in the time-domain (only the zero harmonic component is addressed), whereas the full spectrum of different signals is managed by a multi-rate version of the envelope-oriented HB algorithm, not suffering from bandwidth restrictions (as the standard envelope-oriented HB does).

B. Transmitter co-design for EM-based figures of merit

The computer-aided design (CAD) tools considered in the above subsection can be used to define overall system performance indexes (e.g., in place of the ordinary front-end gain) allowing the power density of the radiated/incident field to be directly related to the signal power flowing in the circuits [40], thus encompassing radiation and nonlinear performance. According to this approach, the system engineer can directly address the goals on the radiating performance of the transceiver.

In this perspective, the first step to be realized is the evaluation of the far-field actually sustained by the nonlinear regime of the transceiver, when operating as a transmitter. As a representative case, Fig. 3 shows the circuit description, according to the PHB principle, of a transmitting front-end with one single-port antenna. For any exciting source level and format, the far-field transmitted by the system, at the generic harmonic F_k, can be evaluated in a straightforward

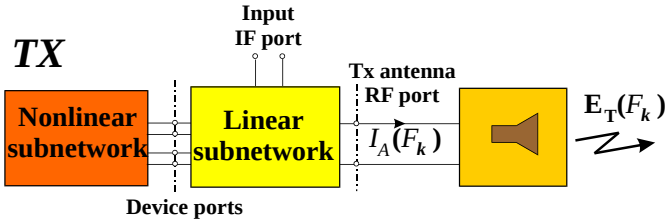

Fig. 3. Radiating transmitter scheme according to the Piecewise HB technique.

way by exploiting the antenna linearity property: in fact, after carrying out the multi-tone HB analysis of the circuit, loaded by the dispersive EM-based description of the antenna (i.e. broadband scattering parameters), the actual current phasor $I_A(F_k)$ obtained after solving (2), and representing the true antenna excitation at the frequency F_k is available, and allows to calculate the far-field, in a spherical reference system (r, θ, ϕ), according to the following formula:

$$\mathbf{E}_{\mathbf{T}}(r,\theta,\phi;F_k)=\frac{\exp(-j\beta r)}{r}\bullet \\ \bullet\left[\hat{\boldsymbol{\theta}}\,A_\theta(\theta,\phi;F_k)+\hat{\boldsymbol{\phi}}\,A_\phi(\theta,\phi;F_k)\right]I_A(F_k) \quad (5)$$

where $\hat{\boldsymbol{\theta}}$, $\hat{\boldsymbol{\phi}}$ are unit vectors in the θ, ϕ directions, respectively, and A_θ, A_ϕ are the scalar components of the normalized far-field, generated by EM simulation [41] with the antenna excited by a unit-current sinusoidal source of frequency F_k. In case of a digitally modulated IF drive, the far-field envelope transmitted at F_k can be easily evaluated as well: in this case the time-dependent current excitation envelope, derived from the solution of (4), must be adopted in a formula similar to (5) [41]. Of course, in case of sinusoidal RF excitation at f_{RF}, F_k corresponds to f_{RF}.

Once the radiated far-field is available, one can formulate the circuit performance by directly exploiting (5) (or its time-based version). For instance, the design goal of the transmitter of Fig. 3 can be the EM transducer gain (G_{ET}) and the circuit-antenna assembly is optimized as a whole by means of nonlinear/EM design techniques, by imposing a flat behavior of G_{ET} over the frequency band. According to the general definition of the antenna gain, G_{ET} is computed by first defining the reference power density (that is the one associated with the equivalently excited isotropic antenna of unity-gain):

$$\frac{\left\|\mathbf{E}_{\mathbf{Ref}}(r_L,\theta_L,\phi_L;F_k)\right\|^2}{2\eta}=\frac{|U_G|^2}{8R_G}\frac{1}{4\pi r_L^2} \quad (6)$$

where U_G, R_G are the impressed voltage and internal impedance of the RF excitation, respectively, η is the free-space impedance, and r_L, θ_L and ϕ_L are the spherical coordinates of the receiving antenna location. Finally, the combination of (6) and the power density derived from (5) allows to define the EM transducer gain as:

$$G_{ET}=\frac{\left\|\mathbf{E}_{\mathbf{T}}(r_L,\theta_L,\phi_L;F_k)\right\|^2}{\left\|\mathbf{E}_{\mathbf{Ref}}(r_L,\theta_L,\phi_L;F_k)\right\|^2}=\frac{16\pi R_G}{\eta|U_G|^2}\left\|\mathbf{A}(\theta_L,\phi_L;F_k)I_A(F_k)\right\|^2 \quad (7)$$

where **A** is the normalized far-field vector containing the far-field components A_θ, A_ϕ.

The advantage of such EM-based gain definition, is to exploit the knowledge of the power density for any possible receiving antenna location (e.g. (r_L, θ_L, ϕ_L)), thus enabling to select the best one.

C. Receiver co-design with EM-computed RF excitations

Once the actual radiation pattern, sustained by the transmitter nonlinear regime, is known through (5), it can be combined with any suitable channel description in order to obtain the field incident onto the receiving front-end antenna ($\mathbf{E_i}$). A challenging aspect for the accurate analysis of the entire microwave link is to obtain the equivalent circuit representation of this EM phenomenon, in order to compute the receiver circuit in realistic excitation conditions. The rigorous application of EM theory [8], [11], [23] allows to exactly compute the RF excitation(s) of the receiving front-end: according to the reciprocity theorem, as described in Fig. 4 for a one-port antenna, two EM configurations are considered, corresponding to the receiving antenna operating in the receiving (Fig. 4(a)) and transmitting (Fig. 4(b)) modes. In the equivalent circuits of Fig. 4, Y_A denotes the EM-based admittance of the antenna under exam.

Let us consider, for simplicity, the condition of free-space propagation, with the RF source and the receiving antenna of the link of Fig. 4(a) in the Fraunhofer region of each other: in these conditions the incident field $\mathbf{E_i}$ can be considered a uniform plane wave in the receiving antenna location. If $\mathbf{E}_A(r, \theta, \phi, F_k)$ is the far field radiated by the receiver antenna operating in the transmitting mode at F_k, and powered by a voltage source of known amplitude U_G, and internal resistance R_G (Fig. 4(b)), it is possible to rigorously compute the Norton current source, $J_{eq}(F_k)$ equivalent to the RF incident field in the following way:

$$J_{eq}(F_k) = j\left[1+R_G Y_A(F_k)\right]\frac{2\lambda\, r\, e^{j\beta r}}{\eta}\frac{\mathbf{E_A}(r,\theta,\phi;F_k)\bullet\mathbf{E_i}}{U_G} \quad (8)$$

An expression similar to (8) holds in case of a non-conventional link, too, where the two antennas of the link can be in the near-field zone and/or far from the maximum direction condition, as in many IoT scenarios [6]. Of course, a similar procedure can be followed to manage a multi-port antenna (or array) case: the scalar Y_A is replaced by an EM-based matrix and the input admittance element at the p-th antenna port is adopted in (8) for the corresponding p-th equivalent generator evaluation.

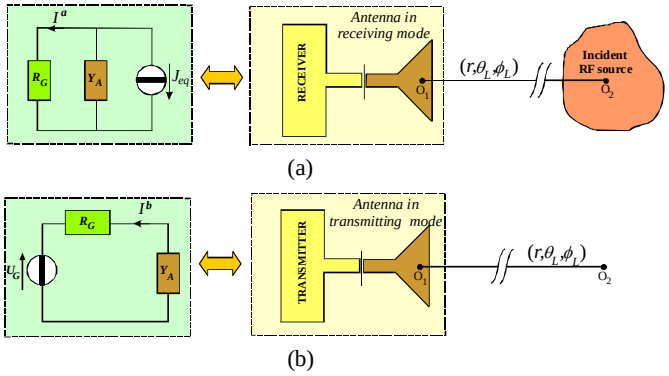

Fig. 4. Exploitation of the reciprocity theorem to compute the actual receiver excitations: (a) Antenna in receiving mode; (b) Antenna in transmitting mode.

It has to be stressed that the inclusion of (8) in the "active" version of the receiver (as reported in Fig. 5) leads to the accurate estimation of both receiver antenna/transmitter antenna and receiver antenna/channel interactions, since no approximations are introduced (e.g. the receiver antenna effective area is not exploited). Furthermore, the polarization mismatch between the receiving antenna and $\mathbf{E_i}$ is automatically accounted for through the scalar product in (8).

The receiver analysis can now be carried out straightforwardly by applying the PHB technique. The adopted equivalent circuit representation of the "active" receiving antenna of Fig. 6(a) is the 3-port network shown in Fig. 6(b), i.e. the parallel connection of two driven current sources, with internal admittance $Y_A(f)$: the two generators are driven by the scalar components of the incoming vector field ($\mathbf{E_i}$) through the transadmittance functions (G_θ, G_ϕ), easily derived from (8). In this figure, **r** represents the point vector (r, θ, ϕ).

The rigorous approach herein described is applicable to a narrowband link, involving the single F_k (typically f_{RF}) carrier transmission [23], [36], as well as a multi-tone excitation. In the latter case, the evaluation of (8) has to be repeated for each incident tone, thus taking into account the receiving antenna(s) radiation patterns at the corresponding frequencies. This is the case of rectifying antennas (rectennas) deploying the multi-(say H) frequency environmental sources simultaneously present in a humanized ambient. Also in this case, the nonlinear rectenna analysis is performed by resorting to the scheme of Fig. 6, where the Norton equivalent current

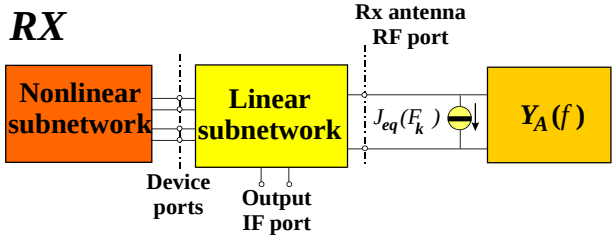

Fig. 5. Schematic block representation of the receiver as an "active" system, according to the Piecewise HB technique.

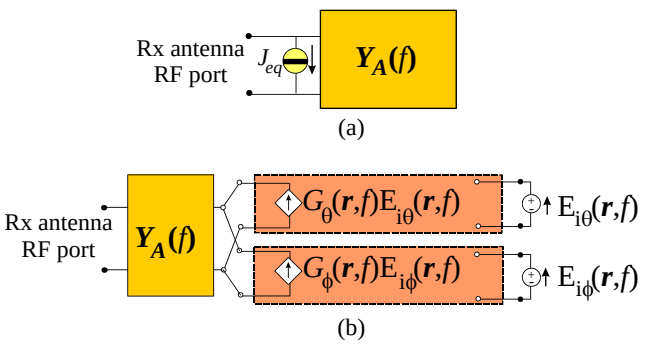

Fig. 6. (a) "Active" receiving antenna scheme derived from EM theory; (b) Its equivalent 3-port circuit representation.

generator is replaced by the parallel of the H current generators evaluated through the application of (8) for each different frequency and link direction [8].

The situation is theoretically identical, simply computationally heavier, in case of Impulse-Radio Ultra-Wide Band (IR-UWB) technology deployment. The use of ultra-short pulses in the communication process, brings to the occupancy of multi-GHz bandwidths: if T_{UWB} is the period of the UWB pulse, the IR-UWB regime can be viewed as a periodic regime of fundamental frequency $f_{UWB} = 1/T_{UWB}$, with a high number (say H_{UWB}) of harmonics for the description of the large frequency band (including higher spectral windows, for nonlinear reasons) [42]. Fig. 7 summarizes these concepts, with the time- and frequency-domain representations of the linear radiating subnetwork: Fig. 7(a) shows a UWB antenna (a Vivaldi one) receiving a short pulse; in Fig. 7(b) the equivalent circuit description is reported with all the needed current generators placed in parallel to the EM-based wide band admittance matrix of the antenna.

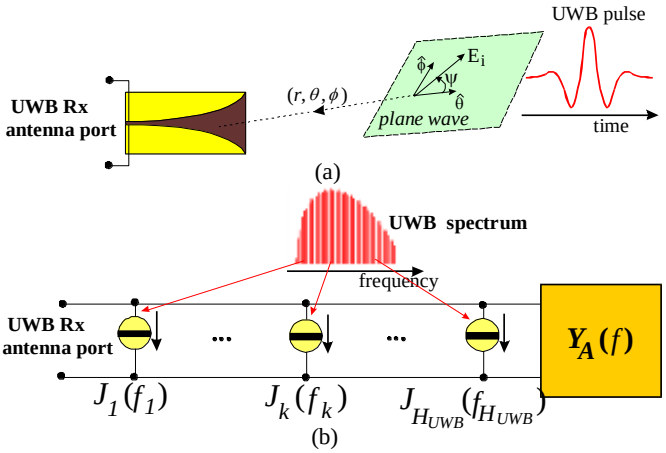

Fig. 7. (a) UWB antenna receiving a IR-UWB time-variable signal; (b) Equivalent "active" scheme of a UWB receiving antenna in frequency domain for HB analysis.

III. UWB Active Transmitting Antenna

A light-weighted UWB travelling wave amplifier (TWA) feeding a slotted monopole UWB antenna is considered as a possible UWB transmitter for localization and tracking applications [43], [44]. It has been designed following the procedure of the subsection II.B and considering, as a major challenge, the optimization of the power transfer, in such a way as to obtain flat received power with minimum ripple

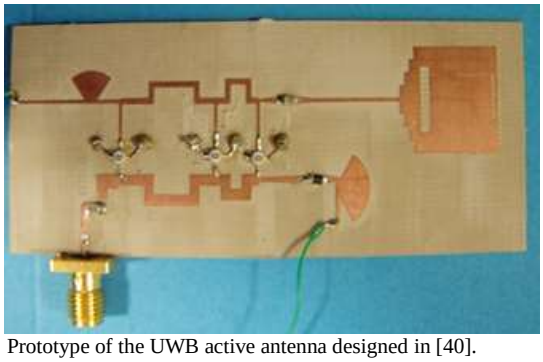

Fig. 8. Prototype of the UWB active antenna designed in [40].

across the very broad frequency band of interest. A photo of the prototype is shown in Fig. 8. The Federal Communications Commission (FCC) band [3.1 – 10.6] GHz was considered and the details on the circuit dimensions are reported in [40]. As NL/EM figure of merit, the transmitter far-field gain G_{ET}, defined in (7), is considered and optimized with the goal of producing a constant radiated power density with limited ripple (lower than 1 dB) all over the FCC UWB band. Such condition is dependent on the combined effect of the amplifier gain, the power transfer between amplifier and antenna, and the antenna gain. Thus, a consistent design allowing the best tradeoff among such quantities needs to be adopted. In addition, EM couplings exist between the antenna and the amplifier, that could influence both the power transfer and the radiation pattern.

As is clear from Fig. 8, there is no electrical output port and the system output is its radiated field computed using (5).

The amplifier-antenna assembly is designed as a broadband nonlinear circuit for a nominal G_{ET} of 10 ± 1 dB at -10 dBm input, with simultaneous specifications at 38 fundamental frequencies uniformly spaced (each every 200 MHz) across the UWB band. In the HB analyses, each regime is accurately described by 4 harmonics plus dc (because of the medium input power level adopted). The design variables are the antenna layout parameters and the widths and lengths of the TWA transmission lines [40]. After the design process, taking about 4 hours on a double-core (Xeon E5-2650, 2 GHz) PC and requiring a total of 37 EM analyses (38 frequencies each), the system has a G_{ET} of 9.5 ± 1.5 dB as shown in Fig. 9, which represents an excellent result for a 3.4:1 band, and an effective control of the gain roll-off at the band edges is observed. In order to provide a quantitative evaluation of the integrated NL/EM co-design effectiveness, the G_{ET} is also calculated starting from the optimization of the standalone amplifier with respect to two different loading conditions, namely a 50-Ohm termination and a complex conjugate load. The simulated results are superimposed in Fig. 9: they both show significant ripple excess with respect to the integrated design.

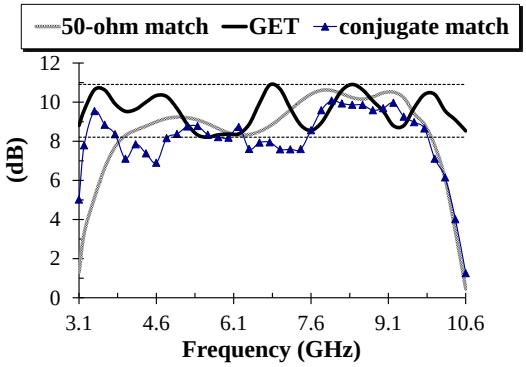

Fig. 9. Computed electromagnetic-transducer gain for different transmitter-antenna system representations [40].

IV. Combined UWB-UHF Tag

This section describes the design of a novel paper-based tag

architecture for next-generation UWB-RFID systems [22], [45], [46]; its block diagram is reported in Fig. 10. The system is designed for backscattering operations, in order to perform ultra-low power communication and localization by means of IR-UWB signals. Furthermore the system is required to be battery-less and, for this reason, it includes a UHF branch for energy harvesting purposes [47]. When dealing with WSN applications, maintenance-free operations can be ensured by means of RF EH and Wireless Power Transfer (WPT) techniques. Typical ambient available power levels, generating from sources such as DTV, GSM and UMTS, hardly exceed 10^{-6}-10^{-4} mW/cm^2 [48], [49], especially in indoor scenarios. Such low amount of available EM energy is often not able to satisfy typical Power Management Units (PMUs) requirements, therefore inhibiting several practical applications. On-demand low-energy powering by means of RF "showers" can be attractive in order to wirelessly provide the minimum energy needed to turn on a distributed number of battery-less microsystems.

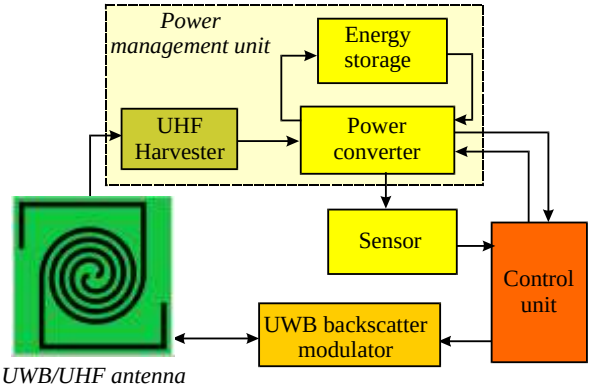

Fig. 10. Schematic view of a novel energy-autonomous microwave system for integrating UWB for localization/communication, and UHF for energy harvesting.

This solution lies somewhere in between conventional EH and WPT systems and it was exploited for the wireless supply of the described tag [4]. The dual-mode (UWB/UHF) operation is realized by a low-profile UWB-UHF antenna and a miniaturized diplexer-like feeding network, located on the back side of the antenna, to enable simultaneous UHF and UWB operations. The full tag design relies on the approach described in Subsection II.C and integrates NL/EM simulations all over the frequency spectra of interest, thus fully taking into account each component contribution to the complete tag operation. This is possible not only for optimizing the UHF and the UWB operations separately, but also for including all the possible coupling between them and their nonlinear effects as well.

One of the peculiar aspect of this tag is the use of only one antenna to cover both the European UHF 868 MHz band and the European low UWB band from 3.1 to 4.8 GHz. This is obtained by exploiting the self-complementary architecture of an Archimedean spiral antenna, which ensures almost constant radiating properties over the UWB whole band. By extension of the spiral outer arms, a compact meandered 1.5-λ dipole is derived with resonance in the 868 MHz band. Besides size

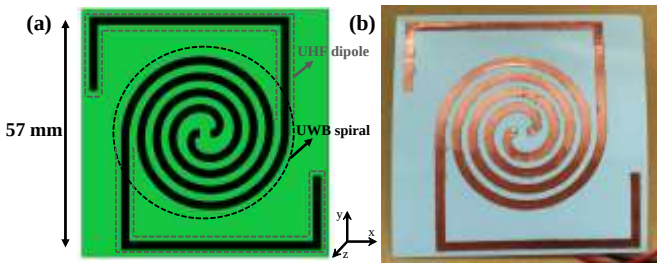

Fig. 11 (a) Integrated UWB-UHF antenna layout; (b) Prototype on paper substrate: with paper thickness 370 μm, ε_r=2.55 and tan(δ)=0.05 @ 24 GHz. The antenna area is 57x57 mm^2.

reduction, co-localization of the two radiating elements leads to a single-port antenna architecture, which is desirable for direct connection to future UWB-UHF integrated chip. The layout of the UWB-UHF antenna is reported in Fig. 11.

For each frequency of interest, thanks to the co-design procedure described in the previous section, the actual antenna complex impedance can be represented strictly, without any need to simplify it with a reference one (50 Ohm termination). Indeed, in the UHF band it is real (10 Ohm only), while in the UWB band it varies between 6 and 37 Ohm, with capacitive reactance. This is shown in Fig. 12 where the comparison between the measured and simulated antenna reflection coefficients is reported: for measurement reasons, the normalization is with respect to the 50 Ohm termination of the Vector Network Analyzer. Hence, the reported graphs are not directly providing the UHF and UWB operating bandwidths. It is noteworthy that this allows to get rid of additional matching components, introducing losses between the antenna and the active sub-system. A direct matching of this complex frequency-dependent behavior to the active sub-circuit is realized by a compact three-port diplexer all over the frequencies of interest. This network, is schematically reported in Fig. 13 (a). It is connected to the antenna by means of two via-holes: one antenna arm reaches the diplexer ground plane, and the other one its input microstrip line. Due to the ungrounded profile of the antenna, the backside diplexer has to guarantee matching and decoupling of the two paths with a miniaturized layout (shown in Figs. 13(b, c)) in order not to

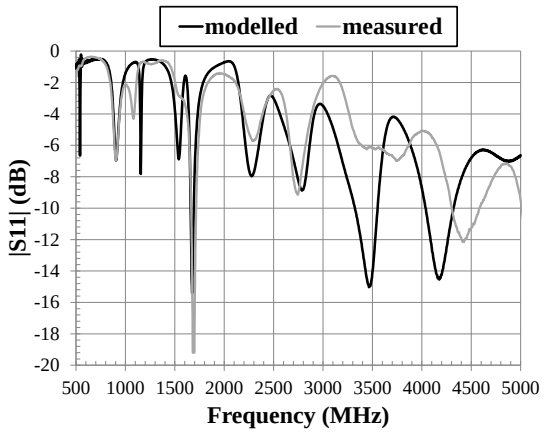

Fig. 12. Modelled and measured integrated UWB-UHF antenna reflection coefficient with respect to 50 Ohm (Vector Network Analyzer reference impedance).

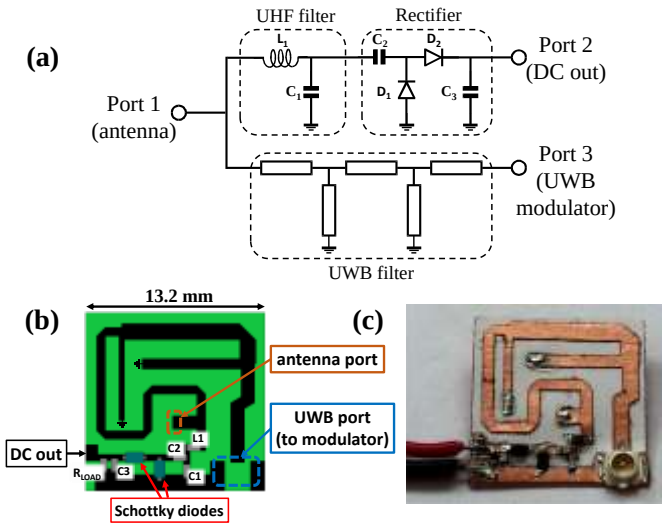

Fig. 13. (a) Circuit schematic of the three-port diplexer with the UHF path connected to a full-wave rectifier (L_1=18 nH, C_1=1 pF, C_2=C_3=10 pF, D_1 and D_2 are the Skyworks SMS7630-079LF Schottky diodes); (b) Its miniaturized layout, 13.2 x 13.2 mm^2; (c) Picture of the prototype on paper substrate.

affect the radiating performance.

Communication in the UWB band is carried out by passive backscattering. For this reason, the diplexer UWB-port will be connected to a backscatter modulator. The modulation of the incident interrogation signal can be implemented by a controlled switching of the UWB load between the two conditions of open and short circuit terminations. For the design of the diplexer, a reference 50 Ohm UWB load has been chosen. In this way, when the tag is inactive, no reflections will occur from the tag if the UWB port is terminated on a 50 Ohm load. An equivalent design procedure can be successfully followed for any other reference impedance.

In the UHF band, the tag operates to provide a rectified dc voltage, converted from the RF signal broadcasted by the RF showers. Such dc voltage can be delivered to a PMU in order to enable additional functionalities of the tag, e.g. sensing, or range extension for the UWB communication. The diplexer UHF path is loaded by a rectifier and optimized in order to reach the highest RF-to-dc conversion efficiency. With this goal, the diplexer network provides direct matching between the antenna UHF impedance and the impedance of the rectifying section, for a specific range of power levels of interest. This is done without recurring to intermediate 50 Ohm matching, thus minimizing the needed circuitry between the antenna and the rectifier and hence the associated losses.

The measured and simulated reciprocal of insertion and return loss are compared in Fig. 14, where the antenna port is replaced by the 50 Ohm termination of the instrument.

The overall double-band design process of the entire antenna-diplexer-rectifier subassembly takes about 3 hours on a double-core (Xeon E5-2650, 2 GHz) PC, including the needed wideband EM simulations.

Fig. 11(b) and 13(c) report the photos of the antenna and diplexer prototypes realized on paper. The adopted fabrication technique is very simple and consists in gluing a copper

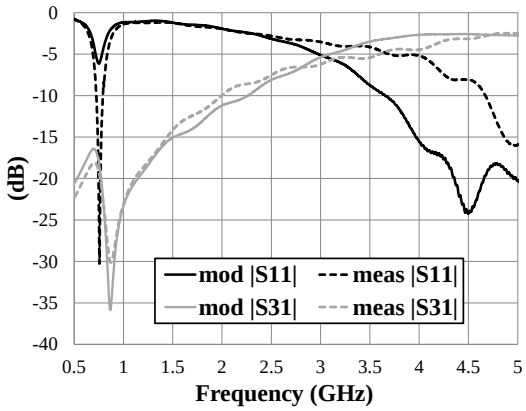

Fig. 14. Comparison between the reciprocal of measured and modelled diplexer antenna port return loss and the antenna-to-UWB port insertion loss. Both UWB port and antenna port are referred to 50 Ohm terminations.

adhesive tape, etched by means of a conventional photo-lithographic process, onto the paper substrate, as described in [50]. This procedure is employed for all the tag metallization layers. Via-through junctions, which connect the antenna to the diplexer, have been realized by means of 0.4 mm-thick copper wires. Finally, diplexer SMD components (with 0402-package) soldering has been realized with the aid of conductive paste, at temperatures below 300° C, in order not to damage the paper substrate.

V. UWB-UHF System Performance

This section is dedicated to discuss the results obtained by the procedure described in section II.C for the design of the integrated UWB-UHF tag, in terms of EH at UHF and backscattering communication in the UWB band. It is shown that the mutual influence of the two operations can be straightforwardly predicted by described co-design process and this is validated by specific measurements.

A. UHF Tag Performance

Tag harvesting capabilities are tested by connecting the antenna/diplexer UHF output port with the rectifier, as detailed in the previous section. The RF-to-dc conversion efficiency is the figure of merit to characterized the tag EH capabilities. To match the predicted RF power used during the NL/EM design process to the measured one, the power received by the standalone antenna, on a 50 Ohm load, is first measured for a fixed distance and orientation of the transmitting UHF antenna. The mismatch loss factor, with respect to the actual antenna impedance, is used to estimate the available RF power at the diplexer input. The measurement has been carried outside an anechoic chamber, in different indoor scenarios, in order to realistically evaluate the RF energy incidence at the tag locations.

In a second step the entire tag is used for the same condition of the transmitting antenna and the DC rectifier output voltage on the optimized load (8 kOhm) is recorded. The comparison between the predicted EM-based nonlinear results and the measured ones, in terms of RF-to-dc conversion efficiency, are superimposed in Fig. 15, for a wide range of input RF

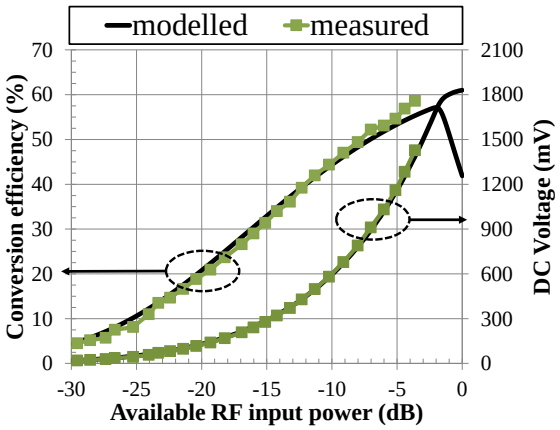

Fig. 15. RF-to-dc conversion efficiency and rectified voltage on the optimum load of 8 kOhm for typically available RF input power levels.

power, from -30 to 0 dBm. The corresponding rectified voltages on the optimum load are also superimposed on the same plot. This test campaign, has been repeated for all the possible loading conditions of the diplexer UWB port (i.e. open-circuit, short-circuit or 50 Ohm) to confirm the optimized decoupling between the UHF and the UWB operations of the tag. For an available input power as low as -10 dBm, the UWB-UHF tag is able to provide a dc power of 44.8 μW and a dc voltage of 600 mV. Such quantities are well suitable to activate the ICs of the UWB path for localizing and addressing the paper tag [4].

B. Computation of the UWB Pulse Distortion received by the antenna

The procedure also allows to predict in a straightforward way the received UWB pulse spectrum and the associated contributions to its amplitude and phase distortion. From the system point of view, this information is fundamental when Time Difference of Arrival (TDOA) techniques are adopted for localization purposes [43].

To do so a circuit-level analysis of the tag excited by a linearly polarized UWB plane wave, can be straightforwardly carried out. For the present case, the UWB pulse consists of the fourth derivative of a Gaussian pulse, with duration τ_d=300 ps and period T_{UWB}=6 ns, satisfying the emission spectral mask [51]. By the HB-based technique, such pulse is accurately described by a spectrum consisting of a fundamental frequency $f_{UWB}=1/T_{UWB}$=166 MHz, with H_{UWB}=64 harmonics. By resorting to the reciprocity theorem detailed in subsection II-C, it is possible to rigorously compute the signal received at the UWB port.

In this way, for a given polarization of the incident field (angle ψ in Fig. 7), the procedure allows to predict the relationship between a received pulse shape and its Angle-of-Arrival (AOA) and vice-versa. Furthermore, the effect on distortion due to the antenna or to the antenna-diplexer assembly are available as well, after the circuit-level analysis. Comparison among transmitted (ideal) and received (real) pulses are reported in Fig. 16, where the reference coordinate system is the same as in Fig. 7.

It is possible to notice that, besides amplitude distortion, a certain phase delay is observed in all the cases. From Fig. 16(b) it is possible to see that different AOAs cause short delays, the maximum one being 30 ps, reported for θ=10°. In this case the main contribution for such distortion is due to the shape of the antenna radiation pattern along that direction. Fig. 16(c) shows that a much longer delay is obtained if the polarization of the incident UWB field is rotated by 90°, and reaches 70 ps. Such contribution can be attributed to the non-perfect circular polarization provided by the antenna. Finally, Fig. 16(d) shows that the presence and absence of the diplexer introduces a 180° phase shift in the received pulse. This last result is not detrimental, since such phenomenon is commonly solved in practical UWB communication by means of a first reference pulse of known polarity for each transmitted bit. Nevertheless this behavior confirms the need for such a co-design technique to take into account all these significant contributions in the evaluation of the system performance. Moreover, it should be noted that in case of a complete backscatter communication, all these delays are doubled.

It is worth noting that, with the present NL/EM approach,

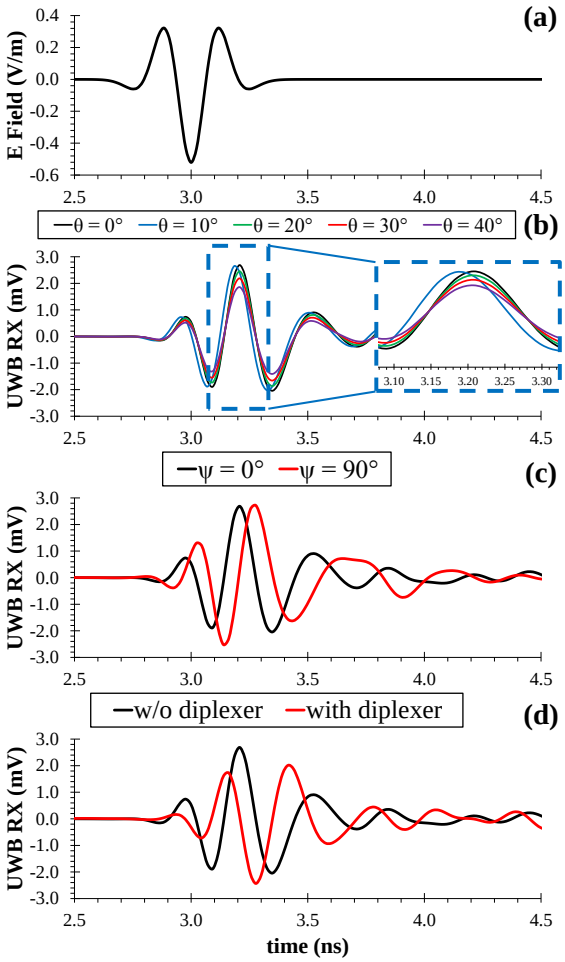

Fig. 16. Antenna distortion effects on the received pulse: (a) UWB pulse incident on the antenna; (b) Received pulse by the stand-alone antenna, for fixed polarization (ψ=0°) and varying elevation θ angle; (c) Received pulse by the stand-alone antenna, for fixed AOA and two different polarizations of the incident field; (d) Received pulse by the stand-alone antenna and the complete tag with the diplexer.

all the effects here discussed can be rigorously taken into account while designing the tag.

As described in [42], the single pulse HB analysis can be extended to the more realistic case of random sequences of pulses (by periodically repeating pseudorandom sequences of a high number of bits), at the expense of a higher computational burden.

C. UWB Tag Measurements

The tag communication capabilities are finally evaluated in a real environment. The measurement set-up consists of a linearly polarized UWB transceiver fed by a Root Raised Cosine generated pulse, with a pulse width factor of 1 ns and roll-off factor 0.6 [44].

With a Pulse Repetition Period set to 50 ns, 200 successive pulses are transmitted and subsequently received by the UWB reader. Such pulses redundancy allows increasing the backscattered energy at the reader side and, therefore, the corresponding Signal-to-Noise Ratio. The received backscattered signal at the reader side is sampled by an oscilloscope and post-processed with a Matlab algorithm [52].

The results, in terms of received power at the reader side, are in Tab. I, where the mean value and standard deviation of 10 consecutive measurements is reported. At a fixed reader-tag distance of 70 cm, the backscatter communication was tested in four different conditions: in the first two the circular polarization capabilities are verified by measuring the received power with two tag positions rotated at 90°; the same two measurements are then repeated in the presence of an UHF RFID reader transmitting a maximum EIRP of +33 dBm, placed at 1.5 m distance from the tag. The successful backscatter communication is obtained which proves that the simulated pulse waveform changes of Fig. 16(c) do not affect the link performance and that, thanks to the integrated design of the whole tag, the nonlinearities of the UHF section do not interfere with the UWB communication capabilities.

Finally, Tab. II reports the UWB link performance for different reader-tag distances for a fixed tag orientation.

TABLE I
RECEIVED POWER BY UWB READER IN DIFFERENT LINK CONDITIONS

Measure	Mean value	Standard deviation
Pol. 1 w/o UHF	-45.7 dBm	0.6 dB
Pol. 2 w/o UHF	-45.4 dBm	0.8 dB
Pol. 1 with UHF	-47.3 dBm	0.6 dB
Pol. 2 with UHF	-46.5 dBm	0.9 dB

TABLE II
RECEIVED POWER BY UWB READER FOR DIFFERENT DISTANCES

Reader-tag distance	Mean value	Standard deviation
50 cm	-41.3 dBm	0.8 dB
70 cm	-45.4 dBm	0.8 dB
90 cm	-50.8 dBm	0.7 dB
110 cm	-52.8 dBm	1.9 dB
130 cm	-57.0 dBm	2.9 dB

VI. CONCLUSION

In this contribution, the main design issues that must be considered for modern RF/microwave micro-systems have been discussed. Such systems need to combine, in a minimum form factor, the antenna, the radio, the sensor, the control logic, and the energy harvesting section. Interconnecting networks among different sub-systems should be avoided, as the main goals are to consume the lowest possible power and to introduce minimum losses. Thus, single component design becomes almost useless or only a starting point for the whole system design. Indeed, it has been showed that, combining state-of-the-art software tools and basic electromagnetic theory, able to systematically handle each subsystem as well as the interactions among subsystems, is the possible way to go. Following the design flow reported in Fig. 17, the key aspects are the EM characterization of the transmit/receive antenna, the analysis of transmit/receive front ends by nonlinear CAD methods, and the description of the EM field as the actual physical link between the transmitter and receiver side. Transmitting and receiving performance of a paper based tag system combing multiple signals for communication and energy harvesting has been used to illustrate the system design approach steps.

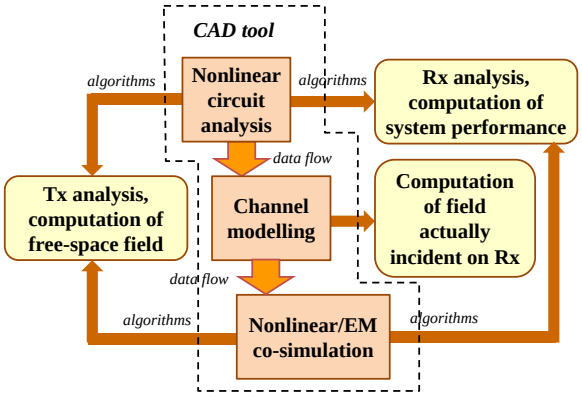

Fig. 17. CAD-based design flow for modern RF/microwave micro-systems.

ACKNOWLEDGMENT

The authors acknowledge their great Mentor and Maestro, Vittorio Rizzoli, who provided them with the foundations for general-purpose and rigorous microwave and RF systems design.

REFERENCES

[1] R. Correia, N.B. Carvalho, and S. Kawasaki, "Continuously Power Delivering for Passive Backscatter Wireless Sensor Networks", *IEEE Trans. Microw. Theory Techn.*, Vol. 64, No. 11, Nov. 2016, pp. 3723 – 3731.

[2] M. Del Prete, D. Masotti, N. Arbizzani, and A. Costanzo, "Remotely Identify and Detect by a Compact Reader With Mono-Pulse Scanning Capabilities", *IEEE Trans. Microw. Theory Techn.*, Vol. 61, No. 1, Part II, Jan. 2013, pp. 641-650.

[3] V. Misra *et al.*, "Flexible Technologies for Self-Powered Wearable Health and Environmental Sensing," *Proceedings of the IEEE*, vol. 103, no. 4, pp. 665-681, April 2015.

[4] N. Decarli *et al.*, "The GRETA architecture for energy efficient radio identification and localization," in *EURFID*, 2015, pp. 1-8.

[5] M. Magno *et al.*, "Design, Implementation, and Performance Evaluation of a Flexible Low-Latency Nanowatt Wake-Up Radio Receiver," *IEEE Trans. Ind. Informat.*, vol. 12, no. 2, pp. 633-644, April 2016.

[6] A. Costanzo, A. Romani, D. Masotti, N. Arbizzani, and V. Rizzoli, "RF/baseband co-design of switching receivers for multiband microwave energy harvesting," *Elsevier Journal on Sensors and Actuators A: Physical*, vol. 179, no. 1, pp. 158-168, March 2012.

[7] T. Paing, E. A. Falkenstein, R. Zane, Z. Popovic, "Custom IC for Ultralow Power RF Energy Scavenging," *IEEE Trans. Power Electron.*, vol. 26, no. 6, pp. 1620-1626, June 2011.

[8] V. Rizzoli, G. Bichicchi, A. Costanzo, F. Donzelli, and D. Masotti, "CAD of multi-resonator rectenna for micro-power generation," in *EuMC*, 2009, pp. 1684-1687.

[9] S. Lemey *et al.*, "Wearable Flexible Lightweight Modular RFID Tag With Integrated Energy Harvester," *IEEE Trans. Microw. Theory Techn.*, vol. 64, no. 7, pp. 2304-2314, July 2016.

[10] E. Falkenstein, D. Costinett, R. Zane, and Z. Popovic, "Far-Field RF-Powered Variable Duty Cycle Wireless Sensor Platform," *IEEE Trans. Circuits Syst. II, Express Briefs*, vol. 58, no. 12, pp. 822-826, Dec. 2011.

[11] A. Georgiadis, G. Vera Andia, and A. Collado, "Rectenna design and optimization using reciprocity theory and harmonic balance analysis for electromagnetic (EM) energy harvesting," *IEEE Antennas Wireless Propag. Lett.*, vol. 9, no. , pp. 444-446, 2010.

[12] H.J. Visser, S. Keyrouz, and A.B. Smolders, "Optimized rectenna design," *Wireless Power Transfer - Cambridge University Press*, vol 2, no. 1, pp. 44-50, 2015.

[13] W. Wiesbeck, G. Adamiuk, and C. Sturm, "Basic Properties and Design Principles of UWB Antennas," *Proc. IEEE*, vol. 97, no. 2, pp. 372-385, Feb. 2009.

[14] A. Costanzo, F. Mastri, D. Masotti, and V. Rizzoli, "Circuit-level nonlinear/EM co-simulation and co-design of UWB receivers," *ICUWB*, 2011, pp. 425-429.

[15] V. Rizzoli, A. Costanzo, D. Masotti, A. Lipparini, and F. Mastri, "Computer-aided optimization of nonlinear microwave circuits with the aid of electromagnetic simulation," *IEEE Trans. Microw. Theory Techn.*, vol. 52, no. 1, pp. 362-377, Jan. 2004.

[16] Xiaolei Ding *et al*., "Neural-network approaches to electromagnetic-based modeling of passive components and their applications to high-frequency and high-speed nonlinear circuit optimization," *IEEE Trans. Microw. Theory Techn.*, vol. 52, no. 1, pp. 436-449, Jan. 2004.

[17] T. J. Brazil, "Nonlinear transient simulation of mixed EM/circuit-level system blocks," *NEMO*, 2014, pp. 1-4

[18] K. Aygun, B. C. Fischer, Jun Meng, B. Shanker, and E. Michielssen, "A fast hybrid field-circuit simulator for transient analysis of microwave circuits," *IEEE Trans. Microw. Theory Techn.*, vol. 52, no. 2, pp. 573-583, Feb. 2004.

[19] H. H. Zhang, L. J. Jiang and H. M. Yao, "Embedding the Behavior Macromodel Into TDIE for Transient Field-Circuit Simulations," *IEEE Trans. Antennas Propag.*, vol. 64, no. 7, pp. 3233-3238, July 2016.

[20] S. Koziel and J. W. Bandler, "Reliable Microwave Modeling by Means of Variable-Fidelity Response Features," *IEEE Trans. Microw. Theory Techn.*, vol. 63, no. 12, pp. 4247-4254, Dec. 2015.

[21] D. Dardari, R. D'Errico, C. Roblin, A. Sibille, and M. Z. Win, "Ultrawide Bandwidth RFID: The Next Generation?," *Proc. IEEE*, vol. 98, no. 9, pp. 1570-1582, Sept. 2010.

[22] M. Fantuzzi, D. Masotti, and A. Costanzo, "A Novel Integrated UWB-UHF One-Port Antenna for Localization and Energy Harvesting," *IEEE Trans. Antennas Propag.*, vol. 63, no. 9, pp. 3839-3848, Sept. 2015.

[23] V. Rizzoli, A. Costanzo, D. Masotti, P. Spadoni, and A. Neri, "Prediction of the End-to-End Performance of a Microwave/RF Link by means of Nonlinear/Electromagnetic Co-Simulation", *IEEE Trans. Microw. Theory Techn.*, Vol. 54, No. 12, pp. 4149-4160, Dec. 2006.

[24] E. Hossain, M. Rasti, H. Tabassum, and A. Abdelnasser, "Evolution toward 5G multi-tier cellular wireless networks: An interference management perspective," *IEEE Wireless Commun.*, vol. 21, no. 3, pp. 118-127, June 2014.

[25] V. Rizzoli, A. Costanzo, D. Masotti, and F. Donzelli, "Integration of numerical and field-theoretical techniques in the design of single- and multi-band rectennas for micro-power generation", *EuMA Int. J. Microw. Wireless Techn.*, vol. 2, No. 3-4, pp. 293-303, July 2010.

[26] D. S. McDowall and V. F. Fusco, "Concurrent large signal simulation of an active microstrip antenna," *Int. J. Numerical Modeling*, vol. 8, no. 1, pp. 3-12, 1995.

[27] K. Liu *et al.*, "Analysis and design of active antenna arrays," in *IMS*, 2001, pp. 1383-1386.

[28] F. Giuppi *et al.*, "X-band cavity-backed slot antennas and coupled oscillator systems," in *EuMC*, 2010, pp. 340-343.

[29] K. S. Kundert and A. Sangiovanni-Vincentelli, "Simulation of Nonlinear Circuits in the Frequency Domain," *IEEE Trans. Comput.-Aided Des. Integr. Circuits Syst.*, vol. 5, no. 4, pp. 521-535, October 1986.

[30] V. Rizzoli *et al*., "State-of-the-art harmonic-balance simulation of forced nonlinear microwave circuits by the piecewise technique," *IEEE Trans. Microw. Theory Techn.*, vol. 40, no. 1, pp. 12-28, Jan 1992.

[31] V. Rizzoli, F. Mastri, F. Sgallari, and V. Frontini, "The exploitation of sparse-matrix techniques in conjunction with the piecewise harmonic-balance method for nonlinear microwave circuit analysis," in *IMS*, 1990, pp. 1295-1298.

[32] N. Soveiko and M. Nakhla, "Wavelet harmonic balance," in *IEEE Microw. Compon. Lett.*, vol. 13, no. 6, pp. 232-234, June 2003.

[33] V. Rizzoli and A. Costanzo, "An accurate bilateral FET model suitable for general nonlinear and power applications," *Int. J. RF Microw. Comput.-Aided Eng.*, vol. 10, no. 1, pp. 43–62, 2000.

[34] V. Rizzoli, R. Gaddi, J. Iannacci, D. Masotti, and F. Mastri, "Multitone intermodulation and RF stability analysis of MEMS switching circuits by a globally convergent harmonic-balance technique", *Proc. European Microwave Association*, vol. 1, no. 1, March 2005, pp. 45-54.

[35] V. Rizzoli, D. Masotti, F. Mastri, and E. Montanari, "System-Oriented Harmonic-Balance Algorithms for Circuit-Level Simulation," *IEEE Trans. Comput.-Aided Des. Integr. Circuits Syst.*, vol. 30, no. 2, pp. 256-269, Feb. 2011.

[36] N. B. Carvalho, J. C. Pedro, W. Jang, and M. B. Steer, "Nonlinear RF circuits and systems simulation when driven by several modulated signals," *IEEE Trans. Microw. Theory Techn.* , vol. 54, no. 2, pp. 572-579, Feb. 2006.

[37] E. Ngoya and R. Larcheveque, "Envelop transient analysis: a new method for the transient and steady state analysis of microwave communication circuits and systems," in *IMS*, 1996, pp. 1365-1368.

[38] D. Sharrit, "New Method of Analysis of Communication Systems", in *MTT-S Nonlinear CAD Workshop*, Jun. 1996.

[39] J. F. Oliveira and J. C. Pedro, "Efficient RF Circuit Simulation Using an Innovative Mixed Time-Frequency Method," *IEEE Trans. Microw. Theory Techn.*, vol. 59, no. 4, pp. 827-836, April 2011.

[40] V. Rizzoli, A. Costanzo, and P. Spadoni, "Computer-Aided Design of Ultra-Wideband Active Antennas by Means of a New Figure of Merit," *IEEE Microw. Compon. Lett.*, Vol. 18, No. 4, pp. 290-292, Apr. 2008.

[41] D. Masotti, P. Francia, A. Costanzo, and V. Rizzoli, "Rigorous Electromagnetic/Circuit-Level Analysis of Time-Modulated Linear Arrays," *IEEE Trans. Antennas Propag.*, vol.61, no.11, pp.5465-5474, Nov. 2013.

[42] V. Rizzoli, F. Mastri, A. Costanzo, and D. Masotti, "Harmonic-Balance Algorithms for the Circuit-Level Nonlinear Analysis of UWB Receivers in the Presence of Interfering Signals," *IEEE Trans. Comput.-Aided Des. Integr. Circuits Syst*, vol. 28, no. 4, pp. 516-527, April 2009.

[43] D. Dardari, A. Conti, U. Ferner, A. Giorgetti, and M. Z. Win, "Ranging With Ultrawide Bandwidth Signals in Multipath Environments," *Proc. IEEE*, vol. 97, no. 2, pp. 404-426, Feb. 2009.

[44] F. Guidi, N. Decarli, S. Bartoletti, A. Conti, and D. Dardari, "Detection of Multiple Tags Based on Impulsive Backscattered Signals," *IEEE Trans. Commun.*, vol. 62, no. 11, pp. 3918-3930, Nov. 2014.

[45] R. Vauche *et al.*, "A remotely UHF powered UWB transmitter for high precision localization of RFID tag," *ICUWB*, 2011, pp. 494-498.

[46] A. Lazaro, A. Ramos, R. Villarino, and D. Girbau, "Active UWB Reflector for RFID and Wireless Sensor Networks," *IEEE Transactions on Antennas and Propagation*, vol. 61, no. 9, pp. 4767-4774, Sept. 2013.

[47] A. Costanzo *et al.*, "Electromagnetic Energy Harvesting and Wireless Power Transmission: A Unified Approach," *Proc. IEEE*, vol. 102, no. 11, pp. 1692-1711, Nov. 2014.

[48] J. A. Hagerty, F. B. Helmbrecht, W. H. McCalpin, R. Zane, and Z. B. Popovic, "Recycling ambient microwave energy with broad-band rectenna arrays," *IEEE Trans. Microw. Theory Techn.*, vol. 52, no. 3, pp. 1014-1024, March 2004.

[49] M. Piñuela, P. D. Mitcheson, and S. Lucyszyn, "Ambient RF Energy Harvesting in Urban and Semi-Urban Environments," *IEEE Trans. Microw. Theory Techn.*, vol. 61, no. 7, pp. 2715-2726, July 2013.

[50] C. Mariotti *et al.*, "Modeling and characterization of copper tape microstrips on paper substrate and application to 24 GHz branchline couplers," in *EuMC*, 2013, pp. 794-797.

[51] http://www.etsi.org/deliver/etsi_en/302000_302099/30206501/01.03.01_60/en_30206501v010301p.pdf.

[52] N. Decarli, F. Guidi, and D. Dardari, "Passive UWB RFID for Tag Localization: Architectures and Design," *IEEE Sensors Journal*, vol. 16, no. 5, pp. 1385-1397, 2016.

Alessandra Costanzo (M'99-SM'13) is associate professor of electromagnetic fields at the University of Bologna, Italy since 2001. Her main research interests include multi-domain design (based on nonlinear/electromagnetic co-simulation) of entire wireless links, such as RF-ID, MIMO and UWB, including rigorous modeling of radiating elements and realistic channel models. Recently she has developed innovative wireless power systems for both far- and near-field solutions. She co-authored more than 150 scientific publications on peer reviewed international journals and conferences and three chapter books; she holds two European and one US patents. She is associate editor of the IEEE Transactions on MTT, of the Cambridge journal of Wireless Power Transfer and of the EuMA International Journal of Microwave and Wireless Technologies. In 2013 she co-funded the EU COST action WiPE "Wireless power transfer for sustainable electronics" where she chairs WG1: "far-field wireless power transfer". Prof. Costanzo is the chair of the IEEE MTT-26 Technical Committee on Wireless Energy Transfer and Conversion, and MTT-S representative of the IEEE Council on RFID.

Diego Masotti (M'00-SM'16) received the Ph.D. degree in electric engineering from the University of Bologna, Italy, in 1997. In 1998 he joined the University of Bologna as a Research Associate of electromagnetic fields. His research interests are in the areas of nonlinear microwave circuit simulation and design, with emphasis on nonlinear/ electromagnetic co-design of integrated radiating subsystems/systems for wireless power transfer and energy harvesting applications. Dr. Masotti serves in the Editorial Board of the International Journal of Antennas and Propagation and of the Cambridge journal of Wireless Power Transfer, and is a member of the Paper Review Board of the IEEE TRANSACTIONS ON MICROWAVE THEORY AND TECHNIQUES since 2004.

Marco Fantuzzi received the B.Sc. degree from the University of Modena and Reggio Emilia, Modena, Italy, and the M.Sc. degree (*magna cum laude*) from the University of Bologna, Bologna, Italy, in 2010 and 2013, respectively.

He joined the Department of Electrical, Electronic and Information Engineering of the University of Bologna in 2014, where he is currently working toward the Ph.D. degree.

His research interests include the design of RF energy harvesting and Wireless Power Transfer systems, as well as RFID technologies and UWB systems.

Massimo Del Prete received the B.S. and M.S. degree in telecommunication engineering at the University of Bologna, Italy, in 2007 and 2011, respectively. In 2014 he joined the Department of Electrical, Electronic and information Engineering, University of Bologna as a PhD student. His research interests include wearable and multi-band antennas, CAD of microwave integrated circuits, with special emphasis on low-power rectenna, power management for autonomous sensors, and wireless power transmission.